Exploration of Sustainable Beam Design Using Voronoi Patterns in Concrete 3D Printing

Gokul Santhosh S[1], Benny Raphael[2], Manu Santhanam[2]

[1]Ph.D. Research Scholar, Building Technology and Construction Management Division, Dept. of Civil Engineering, IIT Madras, Chennai 600036, India
[2]Professor, Building Technology and Construction Management Division, Dept. of Civil Engineering, IIT Madras, Chennai 600036, India
ce22d002@smail.iitm.ac.in, benny@civil.iitm.ac.in, manus@civil.iitm.ac.in

Abstract –

The emergence of concrete 3D printing presents a transformative opportunity for decarbonizing the construction industry by enabling innovative design solutions that prioritize material efficiency and sustainability. While 3D-printed lattice beams have demonstrated significant material reductions using conventional, repetitive patterns, nature-inspired shapes have not been explored. This study investigates the potential of nature-inspired Voronoi patterns for material-efficient concrete beams. Their performance is compared with traditional Truss patterns for symmetrical and unsymmetrical loading conditions. A parametric design system integrated with a genetic algorithm is used to generate various infill patterns for 3D-printable beams. Beam dimensions, orientations, and configurations are optimized while ensuring adequate structural performance. The findings confirm the feasibility of using nature-inspired Voronoi patterns in concrete 3D printing and demonstrate substantial material savings. This approach not only reduces embodied carbon in construction but also enables innovative architectural designs.

Keywords –

Concrete 3D Printing; Voronoi; Shape Optimization; Nature-inspired patterns

1 Introduction

The construction industry is one of the major contributors to carbon emissions, with CO_2 from cement production reaching a staggering 2.9 billion tons in 2021 [1], [2]. Traditional construction methods, which have long dominated the sector, are increasingly unable to meet the growing economies' demands and satisfy sustainability goals at the same time. As a result, optimizing construction processes and materials is crucial for advancing sustainable practices and meeting modern-day demands within the industry.

Additive manufacturing, particularly concrete 3D printing, is emerging as a transformative technology with the potential to address these challenges. By eliminating the need for formwork and enabling direct use of CAD files for construction [3], concrete 3D printing offers significant cost savings, particularly in formwork materials, which typically account for 25-30% of total structural construction costs [4]. Beyond economic benefits, this technology also provides architects and engineers with unprecedented design flexibility, enabling the creation of complex and unconventional geometries that would be difficult or impossible to achieve using traditional methods.

The technology is rapidly advancing, fueled by ongoing research aimed at improving efficiency and broadening adoption. Early studies in concrete 3D printing focused on developing printing technologies [5], [6], optimizing printable mix designs with specific rheological properties [7], [8], integrating supplementary cementitious materials (SCMs) for sustainability [9], and investigating the impact of print parameters on material properties. However, most research has centered on vertical structural elements, such as columns and wall panels, with little attention given to horizontal members [10]. These horizontal elements, such as beams, represent around 43% of the material used in reinforced concrete construction [11]. To further advance concrete 3D printing, research must shift towards optimizing these horizontal, flexural members for improved material efficiency.

Some studies have explored innovative approaches to 3D printing beams. For instance, one method involved assembling smaller units with rebars to print beams, like the process for printing columns [12]. However, this modular approach doesn't fully capitalize on the advantages of 3D printing. Other research focused on optimizing beam structures by printing hollow boundaries and filling them with concrete conventionally [13], but this also fails to maximize the benefits of 3D concrete printing. Recent studies have tested the bending performance of 3D-printed lattice beams with various patterns, showing that triangular lattice beams offer superior performance [14]. Yet, these studies typically use fixed lattice configurations and do not incorporate shape-optimized geometry, which would have further enhanced material efficiency and load-bearing performance.

One promising approach to optimizing 3D-printed beams involves using shape optimization techniques to minimize material usage while maximizing flexural strength. Prior studies have demonstrated the potential of shape-optimized 3D-printed reinforced concrete beams [15], but scalability remains a challenge, particularly as load complexity increases. To make concrete 3D printing a viable solution for large-scale construction, further research is needed to develop optimized, scalable beam designs with a high strength-to-weight ratio.

Structural optimization plays a key role in improving material efficiency, but the complexity of optimized geometries can pose challenges for traditional construction methods, especially when it comes to fabricating formwork. Concrete 3D printing, with its ability to produce complex geometry, aligns well with structural optimization, enabling more sustainable and efficient architectural designs. Nature, with its inherent resource efficiency, has long been a source of inspiration for optimization strategies in materials and structures [16]. However, applying nature-inspired designs in conventional construction has been limited by practical challenges. Concrete 3D printing, on the other hand, is uniquely suited to implement nature-inspired principles, offering the potential to enhance structural efficiency, reduce material usage, and expand the variety of possible constructions [17].

One example of a nature-inspired pattern suitable for 3D-printed lattice beams is the Voronoi pattern, a tessellation often found in nature (e.g., giraffe skin, dragonfly wings, soap bubbles). Previous research has explored the use of Voronoi patterns to optimize the tensile strength of porous structures through genetic algorithms, suggesting potential applications in structural materials [18]. Some parametric studies on 2D rectangular beams with Voronoi tessellations have examined the effects of cell sizes, uniformity, and support conditions on load-carrying capacity [19].

However, the application of Voronoi patterns in concrete 3D printing has not yet been explored. While fabricating Voronoi lattice beams using traditional construction methods would present challenges, concrete 3D printing offers a more feasible and promising approach. Traditionally, Truss patterns have been favoured for their efficiency in load distribution and ease of mass production due to their modularity, whereas the potential of Voronoi patterns remains untapped, mainly in this context.

2 Objectives

The primary objective of this study is to explore the material savings potential of shape-optimized lattice beams featuring Voronoi cell patterns and compare them against the conventional Truss pattern and a regular solid beam for both symmetrical and unsymmetrical loading scenarios.

3 Methodology

The potential for material savings is assessed by comparing various geometric configurations of lattice beams, each individually optimized for shape. 3D-printable lattice beams with different infill patterns are created using a parametric design system and optimized via a genetic algorithm. The system adjusts the geometric parameters within defined limits, and each design is analyzed using finite element software. The sizes of the beam members are determined based on the forces from the analysis, ensuring that all relevant constraints are met. Subsequent sections provide further details on the methodology adopted.

3.1 Geometric Modelling

The study compares beams with two distinct lattice patterns—Truss and Voronoi—against a conventional rectangular beam for both symmetrical and unsymmetrical loading scenarios to assess material efficiency under similar constraints. The beams are modelled as assemblies of line elements representing the edges of the lattice structures. Each lattice type includes multiple variants generated through a combination of parameters. Adopting a parametric modelling approach eliminates the need for manual creation of each variant, enabling efficient exploration of a large design space. The parametric model is implemented using Rhinoceros3D, Grasshopper3D, and Python.

A 6 m span beam is used as a case study to perform the comparative evaluation, with the length-to-depth (l/d) ratio varied between 2 and 20. In addition to the self-weight of the beam, for the symmetrical loading condition, a uniformly distributed load (UDL) of 5 kN/m is applied on the beam's top surface (Figure 1), while for the unsymmetrical loading condition, a point load of 10 kN at 1.5 m from the left support along with a UDL of 5 kN/m running across the full span is applied (Figure 2). The support conditions taken for the study are fixity at both ends. The beam's bottom profile can take either a convex or concave shape, depending on “arc – midpoint offset” parameter. The beam bottom is modelled as a three-point arc with the arc-midpoint offset defining the offset of the midpoint on the arc. The minimum offset is restricted to 10 cm from the midpoint of the beam to facilitate printability. The first and last points of the three-point arc are dependent on the l/d ratio adopted. The depth of the beam at the center changes depending on the offset position of the arc's midpoint, which can range from 0 to 7 meters in steps of 0.1 meters. The thickness and width of all elements are kept constant for a given configuration, where an element represents the connectivity between two nodes. The element dimensions are calculated within specified ranges of the respective parameters, provided in Table 1 and Table 2 for the two lattice beam configurations, ensuring the internal forces remain within specified stress limits. To facilitate thorough design exploration, the starting and ending values of each parameter are deliberately set far apart. These ranges are later verified to confirm that they do not constrain the optimization process.

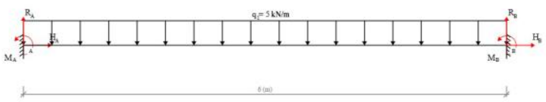

Figure 1. Symmetrical Loading Scenario

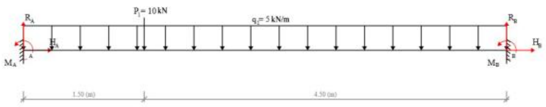

Figure 2. Unsymmetrical Loading Scenario

Table 1. Truss Beam

Sl no	Input parameters	Start Value	End Value	Total Possible Values
1	l/d (ratio)	2	20	19
2	Arc - midpoint offset (m)	-7.0	0.0	71
3	Truss Divisions	5	50	46
4	Thickness (cm)	1	20	20
5	Width (cm)	10	100	91

Table 2.Voronoi Beam

Sl no	Input parameters	Start Value	End Value	Total Possible Values
1	l/d (ratio)	2	20	19
2	Arc - midpoint offset (m)	-7.0	0.0	71
3	Voronoi Count	12	100	89
4	Voronoi Seed	0	1000	1001
5	Thickness (cm)	1	20	20
6	Width (cm)	10	100	91

3.2 Numerical Study

3.2.1 Optimization

Due to the impracticality of manually exploring all possible parameter combinations, a genetic algorithm was employed to optimize the beam configurations for each case, enabling a more efficient identification of the optimal design. Wallacei software, an evolutionary engine for Grasshopper3D, was used for this purpose [20]. Wallacei utilizes the NSGA-2 algorithm [21] as its primary evolutionary algorithm and applies the K-means clustering method. To determine suitable values for population size and the number of generations, multiple trials were conducted with varying parameters, and combinations leading to convergence were identified.

Practical constraints, such as the minimum and maximum lengths of Voronoi edges and cell sizes, were accounted for by defining a range for Voronoi numbers. These constraints were enforced using a penalty function that combines step and ramp components (Figure 3). Penalty functions assign penalty values to solutions that violate constraints, with the penalty magnitude proportional to the degree of violation. The ramp function helps steer the optimization process by gradually reducing constraint violations, while the step function sharply differentiates the feasible design space by assigning high fitness values to feasible regions and penalizing boundary regions with violations. This approach discourages solutions with significant constraint violations, ultimately guiding the optimization toward feasible solutions. Over time, this ensures convergence to designs that fully satisfy all constraints.

To prevent premature convergence to local optima, the genetic algorithm maintains variation within the population. This diversity is introduced using random seed points, with the Voronoi beam utilizing up to 1000 seed points. A higher number of seed points broadens the range of potential configurations, enhancing spatial adaptation under the applied loading conditions. However, increasing the seed points also significantly raises computational power requirements.

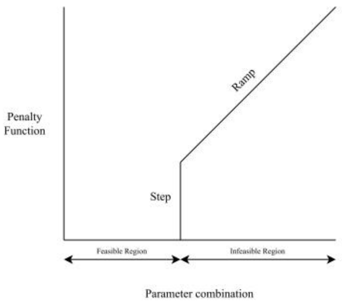

Figure 3. Step and Ramp Function

3.2.2 Implementation Details

The Voronoi pattern was generated using the Voronoi module in Grasshopper3D, based on specified values for the parameters Voronoi seed and Voronoi count. The generated Voronoi was trimmed to fit within the beam's defined boundaries. All parametrically generated line elements were converted into 2D beam elements for structural analysis. This analysis was carried out using Karamba3D [22], a structural analysis plugin for Grasshopper that integrates seamlessly with the parametric modelling approach adopted in the study.

The fixity conditions at the beam's supports were enforced by applying constraints to the nodal points at both ends. A custom Python script was developed to identify the node numbers at these locations and impose the necessary boundary conditions whenever the parametric model was updated during the genetic algorithm's execution.

The beam elements were assigned Material C30/37, compliant with the EN 206-1:2000 standard [23], as its compressive strength closely matched the concrete print mix used in the study. Strength-based constraints were applied, with a maximum allowable tensile stress of 2 MPa and compressive stress of 20 MPa. These constraints guided the optimization process, as no reinforcement is incorporated in this study.

The genetic algorithm varied the cross-sectional dimensions and orientations of the beam elements to ensure compliance with the stress limits. The primary objective was to determine the most efficient configuration for each lattice type by minimizing weight while satisfying criteria for allowable tensile stress, compressive stress, and displacement.

The large design space, resulting from numerous parameters and their wide range of values, facilitated an extensive and systematic search for optimal solutions.

3.2.3 Optimization Results

The masses of beam configurations for the same span were compared to assess potential material savings. Table 3 and Table 4 present the overall mass and percentage material savings relative to the conventional rectangular beam for each configuration for the symmetrical and unsymmetrical loading scenarios respectively.

Table 3. Overall mass and material savings (%) for symmetrical loading

Sl no	Beam Geometry	Mass (kg)	Material Savings (%)
1	Regular Beam	1350	-
2	Truss Beam	875	35.19
3	Voronoi Beam	761	43.64

Table 4. Overall mass and material savings (%) for unsymmetrical loading

Sl. no	Beam Geometry	Mass (kg)	Material Savings (%)
1	Regular Beam	1892	-
2	Truss Beam	1182	37.53
3	Voronoi Beam	833	55.95

The optimized variants of the Truss and Voronoi configurations are detailed in Table 5 and Table 6, respectively. Figure 4 and Figure 5 illustrate the Voronoi and Truss configurations for symmetrical loading case respectively and Figure 6 and Figure 7 represent the same for unsymmetrical loading respectively.

Figure 4. Optimized Voronoi Configuration for Symmetrical Loading

Figure 5. Optimized Truss Configuration for Symmetrical Loading

Figure 6. Optimized Voronoi Configuration for Unsymmetrical Loading

Figure 7. Optimized Truss Configuration for Unsymmetrical Loading

Table 5. Selected variants of Truss beam configuration

Sl no	Input parameters	Symmetrical Loading	Unsymmetrical Loading
1	l/d (ratio)	5	4
2	Arc - midpoint offset (m)	0	0
3	Truss Divisions	13	16
4	Thickness (cm)	12	7
5	Width (cm)	10	19
6	Mass (kg)	875	1182
7	Displacement (cm)	0.0468	0.0470
8	Maximum Tensile Stress (MPa)	0.192	0.198
9	Maximum Compressive Stress (MPa)	0.319	0.392

Table 6. Selected variants of Voronoi beam configuration

Sl no	Input parameters	Symmetrical Loading	Unsymmetrical Loading
1	l/d (ratio)	4	6
2	Arc - midpoint offset	0	0
3	Voronoi Count	25	18
4	Voronoi Seed	227	885
4	Thickness (cm)	13	19
5	Width (cm)	11	10
6	Mass (kg)	761	833
7	Displacement (cm)	0.0407	0.0498
8	Maximum Tensile Stress (MPa)	0.199	0.190
9	Maximum Compressive Stress (MPa)	0.267	0.495

After optimization, the total mass for the Truss and Voronoi configurations in the symmetrical load case was 875 kg and 761 kg, respectively. This resulted in material savings of 35.19% and 43.64% compared to the regular solid beam. As for the unsymmetrical load case, the total mass for the Truss and Voronoi configurations was 1182 kg and 833 kg, respectively. These values correspond to material savings of 37.53% and 55.95% compared to the regular solid beam.

3.3 3D Concrete Printing

To illustrate the printability of Voronoi patterned lattices, a small-scale Voronoi patterned beam is printed. The mix design used for printing the Voronoi beam incorporates a 45 % partial replacement of cement with a blend of limestone and calcined clay [9], and the corresponding mix design is as detailed in Table 7. Superplasticizers and viscosity-modifying admixtures were added at dosages of 0.6% and 0.1% of the binder, respectively, to achieve a printable consistency. This mix had a flow value of 180 mm, measured using the mortar flow table test with 25 drops, and retained 90% of its workability for 60–90 minutes (open time). The mix achieved a density of 2184 kg/m³ and a compressive strength of 30 MPa. The Voronoi lattice pattern generated was converted to G-code and fed to the 3D printer. The mix was fluid enough to bond well at the joints. Figure 8 shows the small-scale printed Voronoi beam.

Table 7. Mix Design

Material	Quantity (kg/m^3)
Quartz Sand – Grade B, 30-80 Mesh	1139
Ordinary Portland Cement (OPC) – 53 Grade	418
LC2 (Limestone + Calcined Clay in 1:2 ratio)	342
Water	304

Figure 8. 3D printed Voronoi Lattice Beam

4 Discussion

The optimization results reveal that the lattice patterns adopted an arch-shaped bottom soffit for both load cases, which helps improve load redistribution and reduce tensile stress in the concrete. Among the patterns analyzed, the Voronoi configuration shows a higher potential for material savings in both load cases, with much more saving potential for the unsymmetrical loading case. This superior performance can be attributed to the unstructured nature of Voronoi patterns. This illustrates the pattern's flexibility in efficiently distributing material where it is most needed and adapting its geometry to the specific characteristics of the design problem.

Of the six optimization variables in the Voronoi beam, the Voronoi seed variable is inherently random. This randomness introduces a degree of disorder along that axis, which limits the genetic algorithm's ability to optimize the seed value globally. However, the algorithm effectively determines the optimal combination of the remaining variables for a fixed seed value. Thus, in the case of Voronoi beams, increasing the number of iterations can help the algorithm uncover even better solutions, although this improvement comes at the cost of additional computational time.

This study thus adopted a parametric-driven approach to shape and topology optimization to develop efficient beam geometries based on load and support conditions. The approach presented is scalable and can be readily applied to larger spans and more complex loading conditions.

5 Conclusion

This study explored the potential of nature-inspired Voronoi patterns for shape optimization in 3D-printed concrete beams. It compares two modular configurations—Truss and Voronoi patterns—against a standard solid beam for both symmetrical and unsymmetrical loading conditions. The key findings include:

- For the symmetrical loading case of the 6m span beam, the percentage savings in the material by the Truss and Voronoi configurations were 35.19% and 43.64% respectively.
- As for the unsymmetrical loading case, the material savings for the Truss and Voronoi configurations were 37.53% and 55.95% respectively.
- The superior performance of the Voronoi configuration for the unsymmetrical loading case is attributed to its non-uniform, unstructured nature-inspired design, which enables optimal material distribution and geometric orientation tailored to specific design requirements.
- This research provides proof of concept that Concrete 3D Printing can successfully fabricate complex Voronoi patterns—challenging to achieve with traditional formwork—while significantly minimizing material usage.

This study highlights how nature-inspired patterns, made feasible through additive manufacturing methods like Concrete 3D Printing, can advance sustainability goals and address the evolving demands of modern architecture. Due to the limitation of testing, we have conducted only numerical study which will be a limitation; however, it is assumed that the theoretical model will be applicable for structures of any scale. Future research will focus primarily on strategies for optimal reinforcement to further enhance load-bearing performance and incorporate ductile failure mechanisms.

6 Acknowledgements

This project is funded by the Science and Engineering Research Board (SERB), India, through the Grant IMP/2018/000224. The Institute of Eminence Research Initiative Project on Technologies for Low-Carbon Lean-Construction (TLC2) and SBI Foundation also provided financial support for this research. Tvasta Manufacturing Solutions Pvt. Ltd., India is thanked by the authors for their support in providing 3D printers for the study.

7 References

[1] B. Sizirici, Y. Fseha, C. S. Cho, I. Yildiz, and Y. J. Byon, "A Review of Carbon Footprint Reduction in Construction Industry, from Design to Operation," Materials 2021, Vol. 14, Page 6094, vol. 14, no. 20, p. 6094, Oct. 2021, doi: 10.3390/MA14206094.

[2] R. Chaudhury, U. Sharma, P. Thapliyal, and L. Singh, "Available online 4," J Clean Prod, vol. 417, pp. 959–6526, 2023, doi: 10.1016/j.jclepro.2023.137466.

[3] T. Wangler, N. Roussel, F. P. Bos, T. A. M. Salet, and R. J. Flatt, "Digital Concrete: A Review," Cem Concr Res, vol. 123, p. 105780, Sep. 2019, doi: 10.1016/J.CEMCONRES.2019.105780.

[4] Z. Huszár and É. Lublóy, "Examination of the cost ratio of the formwork," Acta Technica Jaurinensis, vol. 14, no. 2, pp. 155–170, 2021, doi: 10.14513/actatechjaur.00598.

[5] J. Chung, G. Lee, and J.-H. Kim, "Framework for technical specifications of 3D concrete printers," Autom Constr, vol. 127, p. 103732, 2021, doi: https://doi.org/10.1016/j.autcon.2021.103732.

[6] F. Lyu, D. Zhao, X. Hou, L. Sun, and Q. Zhang, "Overview of the Development of 3D-Printing

Concrete: A Review," Applied Sciences, vol. 11, no. 21, 2021, doi: 10.3390/app11219822.
[7] A. V Rahul, M. K. Mohan, G. De Schutter, and K. Van Tittelboom, "3D printable concrete with natural and recycled coarse aggregates: Rheological, mechanical and shrinkage behaviour," Cem Concr Compos, vol. 125, p. 104311, 2022, doi: https://doi.org/10.1016/j.cemconcomp.2021.104311.
[8] J. Zhang, J. Wang, S. Dong, X. Yu, and B. Han, "A review of the current progress and application of 3D printed concrete," Compos Part A Appl Sci Manuf, vol. 125, p. 105533, Oct. 2019, doi: 10.1016/J.COMPOSITESA.2019.105533.
[9] B. Shantanu, J. Smrati, and S. Manu, "Criticality of binder-aggregate interaction for buildability of 3D printed concrete containing limestone calcined clay," Cem Concr Compos, vol. 136, p. 104853, Feb. 2023, doi: 10.1016/J.CEMCONCOMP.2022.104853.
[10] B. Raphael, S. Senthilnathan, A. Patel, and S. Bhat, "A review of concrete 3D printed structural members," Front Built Environ, vol. 8, p. 1034020, Jan. 2023, doi: 10.3389/FBUIL.2022.1034020/BIBTEX.
[11] H.-W. Cho, S.-G. Roh, Y.-M. Byun, and K.-S. Yom, "Song-Geun Roh; Young-Min Byun; Kyong-Soo Yom ctbuh.org/papers 662 CTBUH," 2004.
[12] J. J. Assaad, A. A. Yassin, F. Alsakka, and F. Hamzeh, "A Modular Approach for Steel Reinforcing of 3D Printed Concrete—Preliminary Study," Sustainability 2020, Vol. 12, Page 4062, vol. 12, no. 10, p. 4062, May 2020, doi: 10.3390/SU12104062.
[13] S. Maitenaz, R. Mesnil, P. Onfroy, N. Metge, and J. F. Caron, "Sustainable Reinforced Concrete Beams: Mechanical Optimisation and 3D-Printed Formwork," RILEM Bookseries, vol. 28, pp. 1164–1173, 2020, doi: 10.1007/978-3-030-49916-7_110/FIGURES/8.
[14] D. Dey, V. N. Van, H. N. Xuan, D. Srinivas, B. Panda, and P. Tran, "Flexural performance of 3D printed concrete structure with lattice infills," Developments in the Built Environment, vol. 16, p. 100297, Dec. 2023, doi: 10.1016/J.DIBE.2023.100297.
[15] L. Breseghello, H. Hajikarimian, H. B. Jørgensen, and R. Naboni, "3DLightBeam+. Design, simulation, and testing of carbon-efficient reinforced 3D concrete printed beams," Eng Struct, vol. 292, p. 116511, Oct. 2023, doi: 10.1016/J.ENGSTRUCT.2023.116511.
[16] N. S. Ramzy, "Beyond Sustainability, Design for Well-Being: Gaudí's Monument to Nature, Biomimetic Functions with Biophilic Morphology," Journal of Architectural Engineering, vol. 28, no. 1, p. 05021016, Mar. 2022, doi: 10.1061/(ASCE)AE.1943-5568.0000515/ASSET/DAB279F9-EFE2-4656-ABB1-3254D2EB97D0/ASSETS/IMAGES/LARGE/FIGURE18.JPG.
[17] A. Du Plessis, A. J. Babafemi, S. Chandra Paul, B. Panda, J. P. Tran, and C. Broeckhoven, "Biomimicry for 3D concrete printing: A review and perspective," 2020, doi: 10.1016/j.addma.2020.101823.
[18] C.-C. Tung, Y.-Y. Lai, Y.-Z. Chen, C.-C. Lin, and P.-Y. Chen, "Optimization of mechanical properties of bio-inspired Voronoi structures by genetic algorithm," 2023, doi: 10.1016/j.jmrt.2023.08.210.
[19] S. Sehat and A. Khatami, "Parametric study on application of Voronoi patterns in design of 2-D beams," Advances in Structural Engineering, vol. 24, no. 11, pp. 2375–2389, Aug. 2021, doi: 10.1177/1369433221999740/FORMAT/EPUB.
[20] "Evolutionary Engine for Grasshopper3D | Wallacei." Accessed: Feb. 02, 2024. [Online]. Available: https://www.wallacei.com/
[21] K. Deb, A. Pratap, S. Agarwal, and T. Meyarivan, "A Fast and Elitist Multiobjective Genetic Algorithm: NSGA-II," IEEE TRANSACTIONS ON EVOLUTIONARY COMPUTATION, vol. 6, no. 2, 2002.
[22] "Karamba3D." Accessed: Jun. 27, 2024. [Online]. Available: https://karamba3d.com/
[23] "EN 206-1:2000 - Concrete - Part 1: Specification, performance, production and conformity." Accessed: Jan. 17, 2024. [Online]. Available: https://standards.iteh.ai/catalog/standards/cen/af40b93d-23eb-43ae-8880-d6b6c9088325/en-206-1-2000